RESEARCH LETTER

Structural dynamics at the active site of the cancer-associated flavoenzyme NQO1 probed by chemical modification with PMSF

Alice Grieco[1], Miguel A. Ruiz-Fresneda[2] (iD), Atanasio Gómez-Mulas[3], Juan Luis Pacheco-García[3], Isabel Quereda-Moraleda[1], Angel L. Pey[3,4] (iD) and Jose M. Martin-Garcia[1] (iD)

1 Department of Crystallography & Structural Biology, Institute of Physical Chemistry Blas Cabrera, Spanish National Research Council (CSIC), Madrid, Spain
2 Department of Microbiology, University of Granada, Granada, Spain
3 Department of Physical Chemistry, University of Granada, Granada, Spain
4 Department of Physical Chemistry, Unit of Excellence in Applied Chemistry to Biomedicine and Environment, and Institute of Biotechnology, University of Granada, Granada, Spain

A large conformational heterogeneity of human NAD(P)H:quinone oxidoreductase 1 (NQO1), a flavoprotein associated with various human diseases, has been observed to occur in the catalytic site of the enzyme. Here, we report the X-ray structure of NQO1 with phenylmethylsulfonyl fluoride (PMSF) at 1.6 Å resolution. Activity assays confirmed that, despite being covalently bound to the Tyr128 residue at the catalytic site, PMSF did not abolish NQO1 activity. This may indicate that the PMSF molecule does not reduce the high flexibility of Tyr128, thus allowing NADH and DCPIP substrates to bind to the enzyme. Our results show that targeting Tyr128, a key residue in NQO1 function, with small covalently bound molecules could possibly not be a good drug discovery strategy to inhibit this enzyme.

Keywords: cancer; flavoenzyme; human NQO1; PMSF; X-ray crystallography

The human NAD(P)H:quinone oxidoreductase 1 (NQO1), is an intracellular, cytosolic, multifunctional flavoenzyme essential for the antioxidant defense system, stabilization of tumor suppressors, and activation of quinone-based chemotherapeutics [1–3]. In addition, alterations in NQO1 function are associated with a variety of human diseases, including cancer, neurological disorders (Parkinson´s and Alzheimer´s diseases, multiple sclerosis, and schizophrenia), and cardiovascular diseases, which makes this enzyme an attractive

cancer target for drug discovery [4]. NQO1 is a very versatile protein showing a dual functionality in cells as it may act as an enzyme and as protein modulator [or chaperone] with stabilizing properties [3,5,6]. As an enzyme, NQO1 primarily catalyzes the two-electron reduction of quinones and a wide variety of other compounds by a double-displacement mechanism commonly known as "ping-pong" mechanism consisting of: (a) binding and oxidation of the electron donor NADH by FAD that reduces to $FADH_2$ with NAD^+

Abbreviations
ASA, accessible surface area; CTD, C-terminal domain; DCPIP, 2,6-Dichlorophenolindophenol; FAD, flavin adenine dinucleotide; NAD(P)H, nicotinamide adenine dinucleotide phosphate; NADH, nicotinamide adenine dinucleotide; NQO1, NAD(P)H:quinone oxidoreductase 1; PDB, protein data bank; PMSF, phenylmethylsulfonyl fluoride; RMSD, root mean square deviation; SDS/PAGE, sodium dodecyl-sulfate polyacrylamide gel electrophoresis.

leaving the binding site; (b) binding and reduction of the substrate by the $FADH_2$. Steps 1 and 2 are reversibly and competitively inhibited by the strong inhibitor dicoumarol [7]. Besides its enzymatic function, NQO1 acts as a non-enzyme being involved in the binding and stabilization of several tumor suppressors such as p53, p33, and p73α [8,9].

Inhibitors such as dicoumarol, other coumarins, flavones, and curcumin, have been reported to inhibit NQO1 function [5,10,11], being dicoumarol the best characterized of them. Dicoumarol is a strong, competitive inhibitor which binds in the active sites of NQO1, directly blocking access by NAD(P)H [8]. Although dicoumarol has been shown to kill pancreatic cancer cells [12,13], this compound is not an ideal anticancer agent due to its off-target effects which include anticoagulant and mitochondrial "uncoupling" activity [14–18]. Thus, a number of studies have been made on identifying novel molecules, often structurally similar to dicoumarol, which are effective NQO1 inhibitors, but lack most of the negative effects dicoumarol has [14]. Although some of them have been shown to be potential anticancer agents, they all failed in clinical trials due to, for example, pharmacokinetics when administered intravenously [19].

NQO1 is a homodimer of 62 kDa with two identical 31 kDa interlocking protomers each of them containing one molecule of flavin adenine dinucleotide (FAD), which is noncovalently attached to the protein. There are two active sites located at the interface between the two protomers consisting of two domains [the N-terminal domain and a small C-terminal domain (CTD)] involving residues from both polypeptide chains. Crystallographic structures of NQO1 with and without NAD^+ and dicoumarol have shown that NQO1 undergoes local conformational changes in which the active site opens and closes during the catalytic mechanism [20,21]. Despite literature showing inhibitors for the function of NQO1, with dicoumarol as a potent competitive inhibitor of NADH and the most effective by inhibiting pancreatic cancer cells in culture, so far, no NQO1 inhibitors are yet in clinical use [12].

In this study, we report the X-ray crystal structure of the human NQO1 protein at 1.6 Å resolution, which is, to the best of our knowledge, the highest-resolution structure so far solved for this enzyme. The only notable difference in the active site region is the modification of Tyr128, which was found to be covalently bound to a molecule of the inhibitor phenylmethylsulfonyl fluoride (PMSF). It is important to note that, in our structure, the presence of the PMSF molecule was unexpected and was found to be covalently bound to the Tyr128 residue in the active site, a strictly conserved and key residue shown to be a key player in the enzymatic function of NQO1 [8,22–25]. The crystal structure reported here is used to compare the modes of binding of NQO1 to previously reported crystal structures of this enzyme with substrates and inhibitors. Activity assays of NQO1-PMSF confirmed that, unexpectedly, although PMSF is covalently bound to Tyr128, it did not inhibit the activity of the enzyme. This may indicate that Tyr128 may not play an important role in the inhibition mechanism of NQO1. The potential involvement of PMSF in the specific activity of the enzyme is discussed. We have also carried out an analysis of the water molecules in NQO1-PMSF. Our analysis revealed the presence of buried well-ordered water molecules at the homodimer interface. Several clusters of water molecules have been identified throughout the interface. These water molecules establish a complex network of hydrogen bonds acting as lubricant. In the light of these preliminary results, we hypothesized that the presence of interfacial water molecules could be responsible, at least partially, for the high plasticity and cooperativity previously reported for NQO1.

Materials and methods

Expression and purification of human NQO1 protein

Protein expression and purification of human NQO1 were carried out as previously described [26] with some modifications. Briefly, *Escherichia coli BL21* (DE3) cells were transformed with pET46 Ek/LIC plasmid containing the cDNA of human NQO1 and grown overnight in 800 mL of lysogeny broth supplemented with 0.1 mg·mL^{-1} ampicillin (LBA) at 37 °C. This starter culture was diluted in 4 L of new LBA and grown at 37 °C until the optical density at 600 nm reached values between 0.6 and 0.8. Expression was then triggered by the addition of isopropyl-β-D-thiogalactoside at a final concentration of 0.5 mM. Induced cells were further incubated for 4 h at 28 °C, harvested by centrifugation, and resuspended in 40 mL of binding buffer (BB, 20 mM sodium phosphate, 300 mM NaCl, and 50 mM imidazole at pH 7.4) containing 1 mM PMSF, flash frozen in liquid N_2 and stored at −80 °C. The following day, cells were lysed by sonication (3 cycles of 2 min each, alternating 2 s ON/2 s OFF with 2 min rest on ice). Lysate was cleared by centrifugation at 92 700 g at 4 °C for 40 min. The supernatant containing NQO1 was filtered through 0.45 μm filters and subsequently loaded onto immobilized Ni^{2+} affinity chromatography columns (Thermo Scientific™ HisPur™ Ni-NTA resin, Waltham, MA, USA), which was

previously equilibrated with BB. After collecting the flow-through, the column was washed with 20 column volumes (CVs) of BB and eluted with 10 CVs of elution buffer (BB containing 500 mм imidazole). The elute protein was dialyzed against 50 mм K-HEPES at pH 7.4. NQO1 protein was further purified by size-exclusion chromatography using a HiLoad 16/600 Superdex 200 prep grade (GE Healthcare, Barcelona, Spain) using 20 mм K-HEPES, 200 mм NaCl at pH 7.4 containing FAD at a final concentration of 1 mм. Pure protein was concentrated to final concentration of 20 mg·mL^{-1} using 30 kDa concentrators from Millipore (Madrid, Spain), flash frozen, and stored at -80 °C. The purity and integrity of the protein were checked by SDS/PAGE.

Protein crystallization

Crystallization of human holo-NQO1 was carried out using the hanging-drop vapor diffusion method, using 24-well plates and the crystallization conditions reported by Faig et al. [27], with some modifications. Briefly, 3 µL of protein at 15 mg·mL^{-1} was mixed with 9 µL of precipitant solution composed of 0.1 м Tris pH 8.5, 0.2 м Sodium Acetate, 20% polyethylene glycol 3350, and 20 µм FAD. Protein droplets were allowed to equilibrate against 500 µL of precipitant solution in the reservoir chambers at 4 °C. Rod-shaped crystals of about 300 µm in size were obtained after few days. Prior to data collection, the crystals were soaked in a cryoprotectant solution containing the precipitant solution with 20% glycerol, looped, and flash-frozen in liquid nitrogen.

Data collection and structure determination

X-ray diffraction data collection was performed on BL-13 XALOC beamline of the ALBA synchrotron radiation source (Barcelona, Spain) using a wavelength of 0.98 Å and a Pilatus 6M detector. Indexing of the collected datasets was performed with XDS [28] and scaling was done with AIMLESS program [29] from the CCP4 suite package [30], and a fraction of 10% reflections were included in the generated R$_{free}$ set. Phasing was performed using molecular replacement with PHASER [31] using the protein data bank (PDB) code 5A4K [32] as search model. The obtained model was refined using alternate cycles of automated refinement using non-crystallographic symmetry with REFMAC5 [33] and manual inspection was performed with coot [34]. Water molecules were automatically upgraded after each refinement cycle. All figures of the protein structure presented in this manuscript were generated with pymol (Schrödinger LLC, New York, NY, USA). The final refined structure was validated using the wwwPDB Validation Service and submitted to the PDB for deposition with PDB 8OK0.

Identification of buried water molecules

The good resolution of our NQO1-PMSF structure has allowed us to identify a total of 1016 water molecules. Buried water molecules in proteins are those that are structurally isolated from the bulk solvent. The presence of buried water molecules was carefully investigated for our NQO1-PMSF structure as follows. Water molecules simultaneously located within 5 Å of the homodimer, and their solvent accessible surface area (ASA) was calculated using the Lee and Richards algorithm [35] as described previously [36]. All water molecules with ASA values greater than 10 Å^2 were discarded and removed from the structure. ASAs were recalculated, and the set of occluded water molecules was iteratively refined until no further changes in accessibility were observed. For all selected water molecules, the interactions established by the identified water molecules with the protein or even with other water molecules were evaluated using pymol (Schrödinger LLC), which uses the Kabsch and Sander's DSSP secondary structure assignment algorithm [37] considering a maximum cut-off distance of 3.5 Å and a minimum angle of 90° for hydrogen bond formation.

Protein activity assays

The enzymatic activity of NQO1-PMSF was performed under aerobic conditions in 20 mм HEPES pH 7.4 at 25 °C using a Varian Cary 50 (Varian Inc., Palo Alto, CA, USA) spectrophotometer. First, NQO1-PMSF was reduced by mixing the protein at a concentration of 1 nм with NADH at 1 mм at room temperature. The mixture was incubated in plastic quartz cuvettes (1-cm pathlength) for 5 min to ensure NQO1-PMSF was fully reduced. Next, the oxidative half-reaction was measured at room temperature by mixing the reduced enzyme with 25 µм of 2,6-Dichlorophenolindophenol (DCPIP) in the same plastic quartz cuvettes. NQO1-PMSF was tested for activity by a static and kinetic read method in triplicate alongside a "substrate only" negative control. For comparison, the enzymatic activity of NQO1 in the absence of PMSF was carried out in parallel in the same reaction conditions. The initial reaction rates were calculated from the changes in A$_{600nm}$ caused by the reduction of DCPIP and were adjusted to account for any non-enzymatic reactions. In all cases, blanks containing all reaction components except the proteins were determined and subtracted from the reactions.

Results and Discussion

Structure of human NQO1 protein in complex with PMSF

Human NQO1 crystals were crystallized in the monoclinic space group I121 with the unit cell dimensions

a = 107.17 Å, b = 58.93 Å, c = 189.16 Å, α = 90°, γ = 98.93°, and β = 90°, and were seen to diffract beyond 1.4 Å resolution. A total of 2400 images were collected and successfully indexed, integrated, and merged. Two physiological homodimers were found in the asymmetric unit yielding a Matthews coefficient [V_M] of 2.08 Å^3/Da and solvent content of 40.78%. The structure of human NQO1 was solved by molecular replacement using the PDB entry 5A4K of the R139W mutant of NQO1 [32], as a search model without the FAD, water, or ion molecules. The structure was refined at a resolution of 1.6 Å with R_{work} and R_{free} of 20.5% and 24.6%, respectively (Table 1). To the best of our knowledge, the structure reported here is the highest-resolution structure reported to date for NQO1 protein. The final data collection and refinement statistics are given in Table 1.

NQO1 is a physiological homodimer made of two interlocked monomers of 273 residues related by a non-crystallographic two-fold axis of symmetry. Each NQO1 monomer is composed of two domains: a large catalytic domain (residues 1–220) and a small CTD (residues 221–273). It is important to note that residue numbers employed in this paper are those used in PDB 5A4K, which are shifted down by one residue with respect to those in some other publications. The molecular structure could be modeled in the electron density from the N-terminus to the C-terminus without interruptions with excellent stereochemistry (root-mean-square deviation (RMSD) from the ideal of 0.008 Å for bond lengths and less than 1.4° bond angles). Ramachandran diagram places nearly all residues within the favored (96%) and allowed (3.8%) regions, with only 0.2% of them falling into the outlier region. The resulting experimental maps were of excellent quality revealing the presence of the cofactors FAD, as well as other solvent molecules such as 1016 water molecules, sodium acetate, and glycerol. Figure 1A illustrates the two homodimers found in the asymmetric unit. The high quality of the NQO1 structure can be assessed from the electron density maps $2mF_o$-DF_c for the cofactor FAD (Fig. 1B).

Analysis of difference electron density maps of NQO1 revealed an unexplained electron density in the catalytic site next to the hydroxyl oxygen of Tyr128. Figure 1C shows the "mysterious" electron density after the initial refinement steps. In three of the four monomers (chains A, B, and D) of the asymmetric unit, the short distance to the density from the side chain of Tyr128 implies a covalent modification of this residue. Based on the size and shape of the "mysterious" density, it could correspond to a phosphate or sulfate group covalently bound to the hydroxyl oxygen

Table 1. X-ray data collection and refinement statistics. Values for the outer shell are given in parentheses.

	NQO1-PMSF
Data collection statistics	
X-ray source/beamline	ALBA/BL-13 XALOC
Wavelength (Å)	0.98
Temperature (K)	100
Detector	Pilatus 6M
Space group	I121
a, b, c (Å)	107.17, 58.93, 189.16
α, β, γ (°)	90.00, 98.93, 90.00
Resolution range (Å)	50–1.6 (1.60–1.64)
No. of unique reflections	135 910
Completeness (%)	98.3 (94.3)
Multiplicity	6.6 (4.7)
R_{merge}	0.073 (4.931)
Avg. I/σ (I)	9.8 (0.2)
Overall B factor from Wilson plot (Å^2)	26.6
Refinement statistics	
Resolution range (Å)	50–1.6 (1.60–1.64)
No. of reflections, working set	135 910
No. of reflections, test set	15 129
R_{work}/R_{free} (%)	20.5/24.6
No. of non-H atoms	
Protein	8744
Water	1016
Others	344
R.m.s. deviations	
Bond length (Å)	0.013
Bond angles (°)	1.637
Average *B* factors (Å^2)	
All atoms	37.0
Protein	36.5
Water	38.2
Ramachandran plot	
Favored (%)	96
Allowed (%)	3.8
Outliers (%)	0.2
PDB code	8OK0

of the tyrosine and to an additional five or six-membered ring bound to the phosphate or sulfate. Since there is no chemical compound with such structural features in the crystallization cocktail, this extra density must come from the purification procedure. By analyzing all chemicals used in the purification of NQO1, the only one that could match with the "mysterious" density was the PMSF, a sulfonyl fluoride compound used as protease inhibitor in the purification of the protein. Accordingly, the model was modified by replacing the tyrosine with a sulfonyl-tyrosine and adding a five-membered ring. After refinement, no residual density above the 3σ level was left in the difference map (Fig. 1D). POLDER maps of the final model of the Tyr128-PMSF are shown in Fig. 1E, clearly confirming the existence of the covalent bond.
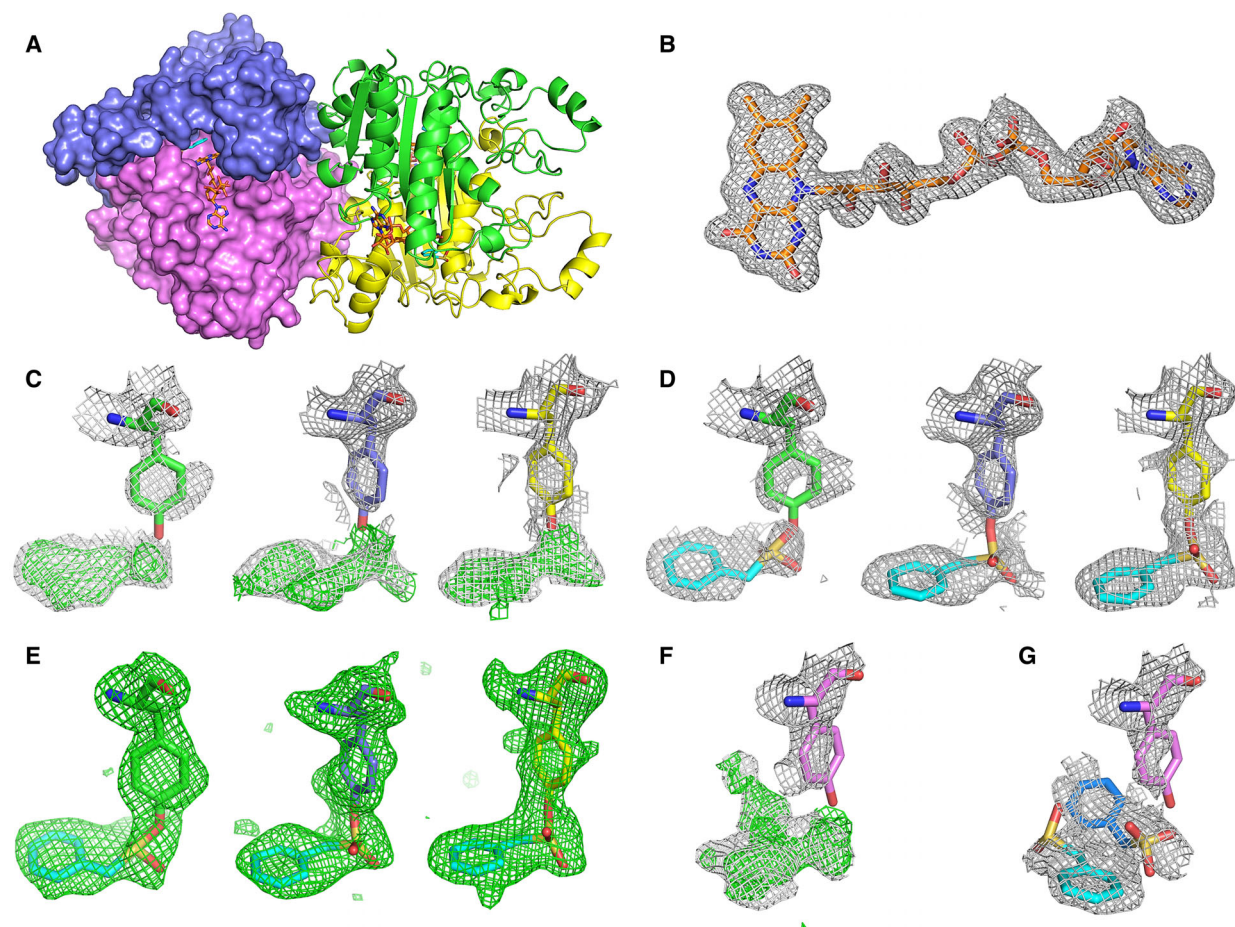
Fig. 1. Crystal structure of human NQO1 in complex with PMSF. (A) Cartoon [chains A (green) and D (yellow)] and surface [chains B (light blue) and C (pink)] representations of the two homodimers of NQO1 found in the asymmetric unit. The cofactor FAD and the PMSF molecules are shown as orange and cyan sticks, respectively. (B) Electron $2mF_c$-DF_o density maps of the FAD molecule contoured at 1σ. (C) Electron $2mF_c$-DF_o (gray) and mF_c-DF_o (green) density maps before refinement contoured at 1σ and 3σ, respectively, around Tyr128 and the "mysterious" molecule in chains A (left), B (middle), and D (right). (D) Electron $2mF_c$-DF_o density maps around Tyr128 and the PMSF molecule after refinement contoured at 1σ in chains A (left), B (middle) and D (right). (E) POLDER maps contoured at 3σ around Tyr128 and the PMSF molecules in chains A (left), B (middle), and D (right). (F) Electron $2mF_c$-DF_o and mF_c-DF_o density maps before refinement contoured at 1σ and 3σ, respectively, around Tyr128 and the "mysterious" molecule in chain C. (G) Electron $2mF_c$-DF_o density maps around Tyr128 and the two PMSF molecules after refinement contoured at 1σ in chain C.

In contrast to chains A, B, and D, the "mysterious" electron density in chain C was broader so that a second molecule of PMSF was modeled. Also, neither of the two PMSF molecules in chain C is covalently bound to Tyr128 (Fig. 1F).

Comparison of human NQO1-PMSF complex with related structures

Further evaluation of the complex NQO1-PMSF structure was carried out by comparing it with previously reported crystal structures of NQO1 both unliganded (PDB 1D4A [21]) and in complex with the natural substrate duroquinone (PDB 1DXO [21]) and various inhibitors such as dicoumarol (PDB 2F1O [8] and 5FUQ (*unpublished work*), Cibacron blue (PDB 4CF6 [38]), various inhibitor molecules (PDBs 1KBO and 1KBQ [39]; PDB 3JSX [18]; and PDB 5EAI [40]), and various chemotherapeutic prodrugs (PDBs 1GG5, 1H66, 1H69 [27]). Overall, all NQO1 structures aligned very well with each other, with RMSD values for all atoms between 0.312 Å and 0.689 Å and with an average value of 0.391 Å. A superimposition of all structures is shown in Fig. 2A. As one could expect, the higher structural differences are mainly found in the loop regions, in the solvent-exposed regions, as
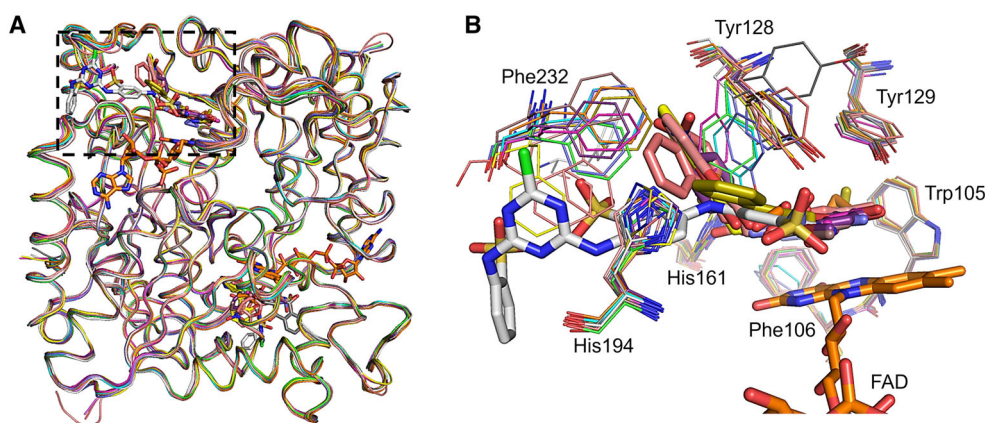
Fig. 2. Structural comparison of the NQO1-PMSF structure with other NQO1 structures. (A) Superimposition of the NQO1-PMSF structure with NQO1 structures both unliganded (PDB 1D4A in cyan [21]) and all liganded structures available to date (PDB 1DXO in pink [21]; PDB 2F1O in yellow [8]; 5FUQ in salmon (*unpublished work*); PDB 4CF6 in white [38]; PDBs 1KBO in brown and 1KBQ in purple [39]; PDB 3JSX in light pink [18]; PDB 5EAI in gray [40]; and PDBs 1GG5 in violet, 1H66 in orange, 1H69 in olive [27]). All protein molecules are represented as ribbons, ligands, and FAD molecules are shown as sticks. The catalytic site is highlighted with a dashed black box. (B) Closer view of the catalytic site highlighted in 'A'. All key residues key for NQO1 function are labeled and represented as thin sticks. All ligands bound to NQO1 are represented as sticks. The FAD molecule is also labeled and represented as orange sticks.

well as in the catalytic pocket where the side chains of several residues show high conformational changes (Fig. 2B). In other words, the binding of PMSF does not alter the overall folding of NQO1 at all.

A further inspection of the catalytic site shows that when there is no ligand bound, the residues Tyr128 and Phe232 are always in a similar conformation. However, the binding of ligands makes the side chains of these two residues move away to accommodate the ligands. In this regard, it has been reported in the literature that NQO1 protein when in its apo state possesses an exceptionally high plasticity and that the binding of either the FAD or dicoumarol reduces it significantly, rigidifying the protein [41–43]. However, this high plasticity has never been seen before structurally until very recently. In a study carried out by our group, we have reported the crystal structure of NQO1 at room temperature using serial crystallography, in which Tyr128 and Phe232 residues have been captured in different conformations within the crystals [44].

We have also carried out a B factor analysis by comparing the B factor of our NQO1-PMSF structure with that of other NOQ1 structures. Although it has clearly been shown that B factors provide useful information about protein flexibility and dynamics, a crucial issue regarding B factors in protein crystal structures is their accuracy. It is well known that B factors are not due to local movements only but reflect additional factors including crystal defects, large-scale disorder, diffraction resolution, and radiation damage.

The latter is particularly intense when using the high flux densities of modern synchrotron sources. It is therefore essential to normalize B factors when comparing different crystal structures. Due to this, and in order to obtain a reliable comparison, from the above-mentioned NQO1 structures, we have selected those structures, both unliganded (PDB 1D4A) and liganded (PDB 1KBQ, 1H66, 1H69, and 5FUQ), that have been determined at resolutions between 1.5 and 2.0 Å. For those structures, we have calculated the normalized B factors as previously reported [45,46] (Fig. S1). See Supplemental Information on how normalized B factors were calculated. Also, for each crystal structure, we have also represented the distribution of the B factors (raw values) across the protein (Fig. S2). From this analysis, it is clear that PMSF molecule seems not to rigidify NQO1 as much as non-covalent inhibitors do.

Mode of binding of PMSF

Although, PMSF has been mainly reported to act as an inhibitor of serine proteases by interacting with the serine nucleophile, there are a couple of studies in which PMSF has also been shown to form covalent bonds with tyrosine residues (see review by Narayanan and Jones [47]). A schematic of the reaction of PMSF with tyrosine residues is shown in Fig. S3.

Until now, all crystal structures reported of NQO1 in complex with ligands, either inhibitor compounds (dicoumarol [8] and Cibacron blue [38]) or

chemotherapeutic prodrugs (RH1, EO9, and ARH019) [27], have shown the ligands non-covalently bound to the protein. In the crystal structure reported in this study, the Tyr128 residue of chains A, B, and D is stabilized by a 1.6 Å long, covalent bond to the sulfate center in PMSF. Thus, the OH functional group of Tyr128 forms o-benzylsulfonyl-tyrosine (Fig. S3). The binding of the inhibitor PMSF buries 300 Å^2 of apolar accessible area of the protein. PMSF binds with its benzyl ring in one side of the pocket, stacked between the Tyr128 residue and the flavin ring of FAD. Tyr128 swings over the inhibitor making a covalent contact with the sulfide atom of the sulphonyl group of the PMSF. PMSF is further stabilized by establishing hydrogen bonds with other residues of the catalytic site such as His161, the FAD molecule and water molecules nearby (Fig. 3).

PMSF does not inhibit the enzymatic activity of NQO1

Neither experimental evidence nor direct structural evidence exists for the binding of PMSF to the active site of NQO1. To confirm whether the activity of the enzyme is diminished or abolished by PMSF, activity assays were carried out as described in Materials and Methods section. Activity assays in kinetic mode were carried out by measuring the reduction of DCPIP by NQO1-PMSF for 5 min (Fig. S4). The initial reaction rates turned out to be 41 ± 9 s^{-1} for the NQO1 in the absence of PMSF and 44 ± 8 s^{-1} for NQO1 with PMSF. Our activity assays confirmed that, although PMSF is covalently bound to Tyr128, it did not abolish the activity of the enzyme. Thus, this may indicate that, unlike expected, Tyr128 may not play an important role in the inhibition mechanism of NQO1. We hypothesize that the high flexibility previously described for this residue is not restricted by the small size of the PMSF molecule so that Tyr128 can still move freely allowing the entrance of the substrates to the catalytic site.

Identification of interfacial water molecules in NQO1-PMSF structure

The presence of interfacial water molecules mediating the interaction between the two protomers at the homodimer interface was investigated. Following the search requirements described in *Materials and Methods*, a total of 1016 water molecules were found (Fig. S5A) in our structure, of which 84 were interfacial buried water molecules (Fig. S5B), 42 water
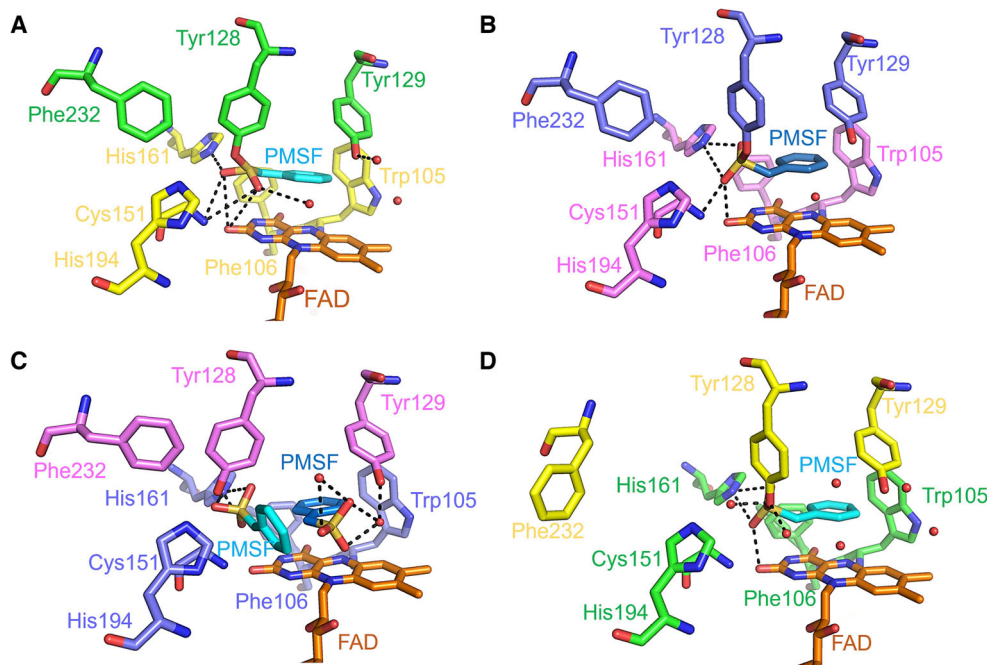

Fig. 3. Binding mode of PMSF molecules in the catalytic sites of NQO1. (A–D) Hydrogen bond interactions (dashed black lines) established by the PMSF molecules with NQO1 residues and water molecules in the catalytic site of chains A (panel A), B (panel B), C (panel C), and D (panel D). The NQO1 residues, the PMSF, and the FAD molecules are labeled and represented as sticks. Waters are represented as red spheres.

molecules per homodimer in the asymmetric unit. These water molecules occupy different hydration sites throughout the homodimer interface (Fig. 4A). The overall properties of these water molecules are shown in Fig. 4B. Overall, most identified interfacial water molecules are significantly buried from the solvent (ASA average = 1.89 Å^2), with nearly 75% of them being characterized by ASA values below 3 Å^2. These molecules are also characterized by B factors that are similar to the average values for protein atoms (36.61 Å), and, in some cases, close to the structure minimum (17.43 Å). Also, these water molecules are implicated in the establishment of multiple specific polar interactions with the protein, with an average of 2.8 hydrogen bonds per water molecule. All hydrogen bond interactions established by the water molecules at the homodimer interface either with other water molecules or protein residues are collected in Tables S1–S4.

Typically, the presence of internal or buried water molecules between the interfaces of protein monomers plays an essential maintenance and stabilizing role.

However, dynamic coupling between protein and hydration water and contributions of buried water molecules to protein plasticity and function have also been extensively studied [36,48–50]. In this regard, several recent studies have reported that the presence of buried water molecules between monomers is associated with protein allostery and cooperativity [51–56]. Thus, from our water molecule analysis in NQO1-PMSF structure, we can hypothesize that the buried water molecules, in addition to stabilizing the homodimer, might be somehow involved in the function of NQO1. Although, we are aware that a more comprehensive study of the water molecules would be needed by comparing NQO1-PMSF to other NQO1 structures available, we believe that the water-buried molecules at the interface act as "lubricant" to favor dynamics and are involved in the plasticity of the NQO1 enzyme as well as play a key role in the negative cooperativity previously described for this protein [23,42,43,57,58]. In fact, an analysis of water molecules along with molecular dynamics simulations is currently being carried out in our labs. Interestingly, we have observed
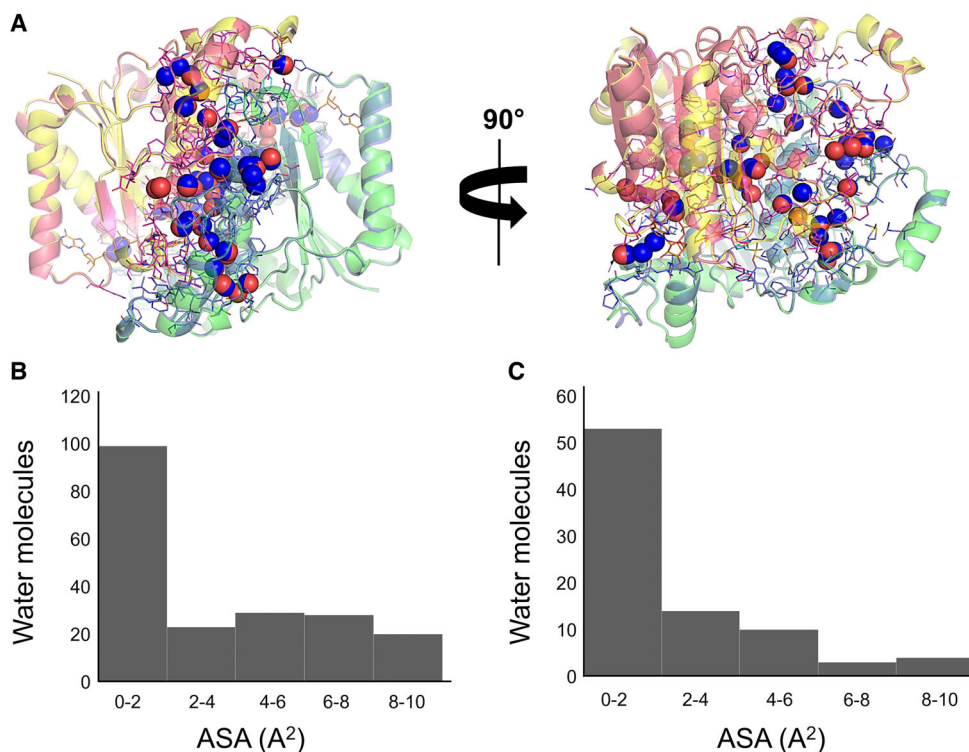

Fig. 4. Buried water molecules in the homodimer interface of NQO1-PMSF structure. (A) Cartoon representation of the two superimposed homodimers of NQO1-PMSF. Homodimers are colored the same as in Fig. 1. Residues at the homodimer interface are shown as sticks. Water molecules are displayed as spheres in red for the homodimer formed by chains A and D, and in blue for the homodimer composed by chains B and C. (B) Solvent accessibility ranges of the total number water molecules identified. (C) Solvent accesibility ranges of the water molecules identified at the homodimer interface.

the presence of water molecules buried at the homodimer interface of all NQO1 structures currently available. The results from this study will be published in a separate manuscript.

Conclusions

This work provides the crystal structure of NQO1 in complex with PMSF inhibitor. The high quality of the data and the nearly high-resolution structure obtained, have allowed us to identify the presence of a high number of buried water molecules. A water molecules analysis identified multiple hydration sites buried at the homodimer interface. This could indicate that the previously reported high plasticity and negative cooperativity of NQO1 [23,42,43,57,58], might be driven by the presence of confined water molecules at the homodimer interface. Furthermore, the analysis of the interactions established by the PMSF molecule at the catalytic site shows PMSF covalently bound to Tyr128 in three of the four monomer chains found in the asymmetric unit. The PMSF benzyl ring is also stacked parallel to the oxacillin ring of FAD. However, unlike expected, the activity assays revealed that the PMSF molecule, despite being covalently bound to Tyr128 residue, does not abolish the catalytic activity of NQO1. This provides us with new insights into the inhibition mechanism of NQO1. Tyr128, which has been reported to be crucial for the function of NQO1 [8,22–25], our results point out that this residue might not play an important role in the inhibition of the enzyme. Therefore, targeting the Tyr128 residue to advance the design of suicide ligands based on sulfonyl fluorinated compounds that could result in new and more potent NQO1 inhibitors by covalently modifying this residue may not be a good strategy unless the new binder establishes other interactions with neighboring residues and thus limiting the dynamics of Tyr128.

Acknowledgements

Author contributions

JMM-G conceived the experiments; JMM-G and ALP designed the experiments; AG, MAR-F, and JLP-G produced the protein; AG, MAR-F, and JMM-G crystallized the NQO1-PMSF protein; AG and MAR-F collected data remotely; JMM-G, AG, and MAR-F solved the structure of NQO1-PMSF; JMM-G and IQ-M performed the water molecules analysis on NQO1-PMSF; ALP, MAR-F, AGM, and JLP-G conducted and analyzed the activity assays; JMM-G, IQ-M, and MAR-F made all figures; JMM-G and ALP wrote the manuscript with input from all other co-authors.

Data accessibility

The protein model coordinates and the associated structure factors of the complex NQO1-PMSF have been deposited in the Protein Data Bank (https:// www.rcsb.org/) with accession code PDB 8OK0. The rest of the data that support the findings of this study are available from the corresponding author (jmmartin@iqf.csic.es) upon reasonable request.

References

1 Pey AL, Megarity CF, Medina-Carmona E and Timson DJ (2016) Natural small molecules as stabilizers and activators of cancer-associated NQO1 polymorphisms. *Curr Drug Targets* **17**, 1506–1514.

2 Ross D and Siegel D (2017) Functions of NQO1 in cellular protection and CoQ10 metabolism and its potential role as a redox sensitive molecular switch. *Front Physiol* **8**, 1–10.

3 Salido E, Timson DJ, Betancor-Fernández I, Palomino-Morales R, Anoz-Carbonell E, Pacheco-García JL, Medina M and Pey AL (2022) Targeting HIF-1α function in cancer through the chaperone action of NQO1: implications of genetic diversity of NQO1. *J Pers Med* **12**, 747.

4 Beaver SK, Mesa-Torres N, Pey AL and Timson DJ (2019) NQO1: a target for the treatment of cancer and neurological diseases, and a model to understand loss of function disease mechanisms. *Biochim Biophys Acta Proteins Proteomics* **1867**, 663–676.

5 Oh ET, Kim JW, Kim JM, Kim SJ, Lee JS, Hong SS, Goodwin J, Ruthenborg RJ, Jung MG, Lee HJ *et al.* (2016) NQO1 inhibits proteasome-mediated degradation of HIF-1α. *Nat Commun* **7**, 13593.

6 Asher G, Tsvetkov P, Kahana C and Shaul Y (2005) A mechanism of ubiquitin-independent proteasomal degradation of the tumor suppressors p53 and p73. *Genes Dev* **19**, 316–321.

7 Anoz-Carbonell E, Timson DJ, Pey AL and Medina M (2020) The catalytic cycle of the antioxidant and cancer-associated human NQO1 enzyme: hydride transfer, conformational dynamics and functional cooperativity. *Antioxidants* **9**, 1–22.

8 Asher G, Dym O, Tsvetkov P, Adler J and Shaul Y (2006) The crystal structure of NAD[P]H quinone oxidoreductase 1 in complex with its potent inhibitor dicoumarol. *Biochemistry* **45**, 6372–6378.

9 Anwar A, Dehn D, Siegel D, Kepa JK, Tang LJ, Pietenpol JA and Ross D (2003) Interaction of human NAD[P]H:Quinone oxidoreductase 1 [NQO1] with the tumor suppressor protein p53 in cells and cell-free systems. *J Biol Chem* **278**, 10368–10373.

10 Siegel D, Harris PS, Michel CR, de Cabo R, Fritz KS and Ross D (2022) Redox state and the sirtuin deacetylases are major factors that regulate the acetylation status of the stress protein NQO1. *Front Pharmacol* **13**, 1015642.

11 Siegel D, Bersie S, Harris P, Di Francesco A, Armstrong M, Reisdorph N, Bernier M, de Cabo R, Fritz K and Ross D (2021) A redox-mediated conformational change in NQO1 controls binding to microtubules and α-tubulin acetylation. *Redox Biol* **39**, 101840.

12 Cullen JJ, Hinkhouse MM, Grady M, Gaut AW, Liu J, Zhang YP, Weydert CJ, Domann FE and Oberley LW (2003) Dicumarol inhibition of NADPH:quinone oxidoreductase induces growth inhibition of pancreatic cancer via a superoxide-mediated mechanism. *Cancer Res* **63**, 5513–5520.

13 Lewis A, Ough M, Li L, Hinkhouse MM, Ritchie JM, Spitz DR and Cullen JJ (2004) Treatment of pancreatic cancer cells with dicumarol induces cytotoxicity and oxidative stress. *Clin Cancer Res* **10**, 4550–4558.

14 Labbe-Bois R, Laruelle C and Godfroid JJ (1975) Quantitative structure-activity relations for dicoumarol antivitamins K in the uncoupling of mitochondrial oxidative phosphorylation. *J Med Chem* **18**, 85–90.

15 López-Lira C, Alzate-Morales JH, Paulino M, Mella-Raipán J, Salas CO, Tapia RA and Soto-Delgado J (2018) Combined molecular modelling and 3D-QSAR study for understanding the inhibition of NQO1 by heterocyclic quinone derivatives. *Chem Biol Drug Des* **91**, 29–38.

16 Bian J, Deng B, Xu L, Xu X, Wang N, Hu T, Yao Z, Du J, Yang L, Lei Y *et al.* (2014) 2-substituted 3-methylnaphtho[1,2-b]furan-4,5-diones as novel L-shaped ortho-quinone substrates for NAD[P]H:quinone oxidoreductase [NQO1]. *Eur J Med Chem* **82**, 56–67.

17 Scott KA, Barnes J, Whitehead RC, Stratford IJ and Nolan KA (2011) Inhibitors of NQO1: identification of compounds more potent than dicoumarol without associated off-target effects. *Biochem Pharmacol* **81**, 355–363.

18 Nolan KA, Doncaster JR, Dunstan MS, Scott KA, Frenkel AD, Siegel D, Ross D, Barnes J, Levy C, Leys D *et al.* (2009) Synthesis and biological evaluation of coumarin-based inhibitors of NAD[P]H: Quinone oxidoreductase-1 [NQO1]. *J Med Chem* **52**, 7142–7156.

19 Phillips RM, Hendriks HR and Peters GJ (2013) EO9 [Apaziquone]: from the clinic to the laboratory and back again. *Br J Pharmacol* **168**, 11–18.

20 Chhetri J, King AE and Gueven N (2017) Alzheimer's disease and NQO1: is there a link? *Curr Alzheimer Res* **15**, 56–66.

21 Faig M, Bianchet MA, Talalay P, Chen S, Winski S, Ross D and Amzel LM (2000) Structures of recombinant human and mouse NAD[P]H:quinone oxidoreductases: species comparison and structural changes with substrate binding and release. *Proc Natl Acad Sci USA* **97**, 3177–3182.

22 Li R, Bianchet MA, Talalay P and Amzel LM (1995) The three-dimensional structure of NAD[P]H:quinone reductase a flavoprotein involved in cancer chemoprotection and chemotherapy: mechanism of the two-electron reduction. *Proc Natl Acad Sci USA* **92**, 8846–8850.

23 Megarity CF, Abdel-Aal Bettley H, Caraher MC, Scott KA, Whitehead RC, Jowitt TA, Gutierrez A, Bryce RA, Nolan KA, Stratford IJ *et al.* (2019) Negative cooperativity in NAD[P]H Quinone oxidoreductase 1 [NQO1]. *ChemBioChem* **20**, 2841–2849.

24 Ma Q, Cui K, Xiao F, Lu AYH and Yang CS (1992) Identification of a glycine-rich sequence as an NAD[P] H-binding site and tyrosine 128 as a dicumarol-binding site in rat liver NAD[P]H:quinone oxidoreductase by site-directed mutagenesis. *J Biol Chem* **267**, 22298–22304.

25 Pandey P, Avula B, Khan IA, Khan SI, Navarro VJ, Doerksen RJ and Chittiboyina AG (2020) Potential modulation of human NAD[P]H-Quinone oxidoreductase 1 [NQO1] by EGCG and its metabolites – a systematic computational study. *Chem Res Toxicol* **33**, 2749–2764.

26 Pey AL, Megarity CF and Timson DJ (2014) FAD binding overcomes defects in activity and stability displayed by cancer-associated variants of human NQO1. *Biochim Biophys Acta – Mol Basis Dis* **1842**, 2163–2173.

27 Faig M, Bianchet MA, Winski S, Hargreaves R, Moody CJ, Hudnott AR, Ross D and Amzel LM (2001) Structure-based development of anticancer drugs: complexes of NAD[P]H:quinone oxidoreductase 1 with chemotherapeutic quinones. *Structure* **9**, 659–667.

28 Kabsch W (2010) XDS. *Acta Crystallogr D Biol Crystallogr* **66** (Pt 2), 125–132.

29 Evans PR and Murshudov GN (2013) How good are my data and what is the resolution? *Acta Crystallogr D Biol Crystallogr* **69**, 1204–1214.

30 Winn MD, Ballard CC, Cowtan KD, Dodson EJ, Emsley P, Evans PR, Keegan RM, Krissinel EB, Leslie AG, McCoy A et al. (2011) Overview of the CCP4 suite and current developments. *Acta Crystallogr D Biol Crystallogr* **67**, 235–242.

31 McCoy AJ (2007) Solving structures of protein complexes by molecular replacement with Phaser. *Acta Crystallogr D Biol Crystallogr* **63** (Pt 1), 32–41.

32 Lienhart W, Strandback E, Gudipati V, Koch K, Binter A, Uhl MK, Rantasa DM, Bourgeois B, Madl T, Zangger K et al. (2018) Catalytic competence, structure and stability of the cancer-associated R139W variant of the human NAD[P]H: quinone oxidoreductase 1 (NQO1). *FEBS J* **284**, 1233–1245.

33 Murshudov GN, Skubák P, Lebedev AA, Pannu NS, Steiner RA, Nicholls RA, Winn MD, Long F and Vagin AA (2011) REFMAC5 for the refinement of macromolecular crystal structures. *Acta Crystallogr D Biol Crystallogr* **67**, 355–367.

34 Emsley P, Lohkamp B, Scott WG and Cowtan K (2010) Features and development of Coot. *Acta Crystallogr D Biol Crystallogr* **66**, 486–501.

35 Lee B and Richards FM (1971) The interpretation of protein structures: estimation of static accessibility. *J Mol Biol* **55**, 379–400.

36 Martin-Garcia JM, Ruiz-Sanz J and Luque I (2012) Interfacial water molecules in SH3 interactions: a revised paradigm for polyproline recognition. *Biochem J* **442**, 443–451.

37 Frishman D and Argos P (1995) Knowledge-based protein secondary structure assignment. *Proteins Struct Funct Bioinform* **23**, 566–579.

38 Lienhart WD, Gudipati V, Uhl MK, Binter A, Pulido SA, Saf R, Zangger K, Gruber K and Macheroux P (2014) Collapse of the native structure caused by a single amino acid exchange in human NAD[P]H: Quinone oxidoreductase. *FEBS J* **281**, 4691–4704.

39 Winski SL, Faig M, Bianchet MA, Siegel D, Swann E, Fung K, Duncan MW, Moody CJ, Amzel LM and Ross D (2001) Characterization of a mechanism-based inhibitor of NAD[P]H:Quinone oxidoreductase 1 by biochemical, X-ray crystallographic, and mass spectrometric approaches. *Biochemistry* **40**, 15135–15142.

40 Pidugu LSM, Mbimba JCE, Ahmad M, Pozharski E, Sausville EA, Emadi A and Toth EA (2016) A direct interaction between NQO1 and a chemotherapeutic dimeric naphthoquinone. *BMC Struct Biol* **16**, 1.

41 Martínez-Limón A, Alriquet M, Lang WH, Calloni G, Wittig I and Vabulas RM (2016) Recognition of enzymes lacking bound cofactor by protein quality control. *Proc Natl Acad Sci USA* **113**, 12156–12161.

42 Encarnación MC, Palomino-Morales RJ, Fuchs JE, Esperanza PG, Noel MT, Salido E, Timson DJ and Pey AL (2016) Conformational dynamics is key to understanding loss-of-function of NQO1 cancer-associated polymorphisms and its correction by pharmacological ligands. *Sci Rep* **6**, 20331.

43 Vankova P, Salido E, Timson DJ, Man P and Pey AL (2019) A dynamic core in human NQO1 controls the functional and stability effects of ligand binding and their communication across the enzyme dimer. *Biomolecules* **9**, 728.

44 Doppler D, Sonker M, Egatz-gomez A, Grieco A, Zaare S, Jernigan R, Meza-Aguilar JD, Rabbani MT, Manna A, Alvarez RC et al. (2023) Modular droplet injector for sample conservation providing new structural insight for the conformational heterogeneity in the disease-associated NQO1 enzyme. *Lab Chip* **23**, 3016–3033.

45 Parthasarathy S and Murthy MRN (1997) Analysis of temperature factor distribution in high-resolution protein structures. *Protein Sci* **6**, 2561–2567.

46 Schlessinger A and Rost B (2005) Protein flexibility and rigidity predicted from sequence. *Proteins Struct Funct Genet* **61**, 115–126.

47 Narayanan A and Jones LH (2015) Sulfonyl fluorides as privileged warheads in chemical biology. *Chem Sci* **6**, 2650–2659.

48 Sterpone F, Stirnemann G and Laage D (2012) Magnitude and molecular origin of water slowdown next to a protein. *J Am Chem Soc* **134**, 4116–4119.

49 Bellissent-Funel MC, Hassanali A, Havenith M, Henchman R, Pohl P, Sterpone F, van der Spoel D, Xu Y and Garcia AE (2016) Water determines the structure and dynamics of proteins. *Chem Rev* **116**, 7673–7697.

50 Schirò G and Weik M (2019) Role of hydration water in the onset of protein structural dynamics. *J Phys Condens Matter* **31**, 463002.

51 Leitner DM, Hyeon C and Reid KM (2020) Water-mediated biomolecular dynamics and allostery. *J Chem Phys* **152**, 240901.

52 Setny P and Wisniewska MD (2018) Water-mediated conformational preselection mechanism in substrate binding cooperativity to protein kinase A. *Proc Natl Acad Sci USA* **115**, 3852–3857.

53 Mustata G and Briggs JM (2004) Cluster analysis of water molecules in alanine racemase and their putative structural role. *Protein Eng Des Sel* **17**, 223–234.

54 Guan X, Tan C, Li W, Wang W and Thirumalai D (2022) Role of water-bridged interactions in metal ion coupled protein allostery. *PLoS Comput Biol* **18**, 1010195.

55 Orgován Z, Ferenczy GG and Keserű GM (2019) The role of water and protein flexibility in the structure-based virtual screening of allosteric GPCR modulators: an mGlu5 receptor case study. *J Comput Aided Mol Des* **33**, 787–797.

56 Royer WE, Pardananii A, Gibson QH, Peterson ES and Friedman JM (1996) Ordered water molecules as key allosteric mediators in a cooperative dimeric hemoglobin. *Proc Natl Acad Sci USA* **93**, 14526–14531.

57 Medina-Carmona E, Neira JL, Salido E, Fuchs JE, Palomino-Morales R, Timson DJ and Pey AL (2017) Site-to-site interdomain communication may mediate different loss-of-function mechanisms in a cancer-associated NQO1 polymorphism. *Sci Rep* **7**, 44532.

58 Pacheco-Garcia JL, Loginov DS, Anoz-carbonell E, Vankova P, Palomino-morales R, Salido E, Man P, Medina M, Naganathan AN and Pey AL (2022) Allosteric communication in the multifunctional and redox NQO1 protein studied by cavity-making mutations. *Antioxidants* **11**, 1110.

Supporting information

Additional supporting information may be found online in the Supporting Information section at the end of the article.

Fig. S1. Normalized B factors as a function of the atom number for the selected protein structures.

Fig. S2. B factor comparison of NQO1 crystal structures.

Fig. S3. Schematic of the reaction of PMSF molecule with Tyr128 residues of NQO1

Fig. S4. Kinetics of NQO1-PMSF re-oxidation by DCPIP.

Fig. S5. Water molecules analysis on NQO1-PMSF.

Table S1. Water–protein interactions at the homodimer interface between chains A/D.

Table S2. Water–protein interactions at the homodimer interface between chains B/C.

Table S3. Water–water interactions at the homodimer interface between chains A/D.

Table S4. Water–water interactions at the homodimer interface between chains B/C.